JACS Au
AN OPEN ACCESS JOURNAL OF THE AMERICAN CHEMICAL SOCIETY

Open Access
This article is licensed under CC-BY-NC-ND 4.0

pubs.acs.org/jacsau
Article

Mechanistic Insight into the Mechanical Unfolding of the Integral Membrane Diacylglycerol Kinase

Huiying Yang, Daihong Zhou, Zhangyi Zhou, Mojie Duan,* and Hao Yu*

Cite This: JACS Au 2024, 4, 1422−1435
Read Online

ACCESS | Metrics & More | Article Recommendations | Supporting Information

ABSTRACT: The essential forces stabilizing membrane proteins and governing their folding and unfolding are difficult to decipher. Single-molecule atomic force spectroscopy mechanically unfolds individual membrane proteins and quantifies their dynamics and energetics. However, it remains challenging to structurally assign unfolding intermediates precisely and to deduce dominant interactions between specific residues that facilitate either the localized stabilization of these intermediates or the global assembly of membrane proteins. Here, we performed force spectroscopy experiments and multiscale molecular dynamics simulations to study the unfolding pathway of diacylglycerol kinase (DGK), a small trimeric multispan transmembrane enzyme. The remarkable agreement between experiments and simulations allowed precise structural assignment and interaction analysis of unfolding intermediates, bypassing existing limitations on structural mapping, and thus provided mechanistic explanations for the formation of these states. DGK unfolding was found to proceed with structural segments varying in size that do not correlate with its secondary structure. We identified intermolecular side-chain packing interactions as one of the major contributions to the stability of unfolding intermediates. Mutagenesis creating packing defects induced a dramatic decrease in the mechano-stability of corresponding intermediates and also in the thermo-stability of DGK trimer, in good agreement with predictions from simulations. Hence, the molecular determinants of the mechano- and thermo-stability of a membrane protein can be identified at residue resolution. The accurate structural assignment established and microscopic mechanism revealed in this work may substantially expand the scope of single-molecule studies of membrane proteins.

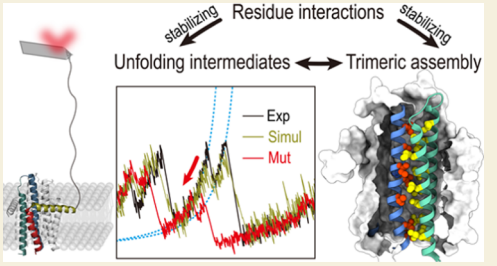

KEYWORDS: *membrane protein folding, single-molecule force spectroscopy, atomic force microscopy, diacylglycerol kinase, unfolding pathway and intermediate, MD simulations*

INTRODUCTION

Membrane protein folding is governed by a delicate balance of various types of interactions between protein residues and the lipid bilayer.[1−6] The amphiphilicity of membrane proteins and their surrounding environment makes them experimentally challenging to study.[4,7] Atomic force spectroscopy (AFM) is inherently suitable to study membrane proteins in near-native artificial lipid bilayers[8−10] or native membranes.[11−15] AFM-based single-molecule force spectroscopy (SMFS) can provide unique insights into mechanisms of folding and function that may be otherwise hidden in ensemble-based methods.[16−20] Mechanical unfolding is typically the first and most basic step in SMFS studies.[21] A wealth of information can be deduced by analyzing the unfolding pathway and quantifying the physical properties of unfolding intermediates.[21] For example, the kinetics and energetics of structural segments can be quantified[14,22−24] and used to fingerprint different functional states[11,14] or understand how these molecular properties respond to ligand binding,[9] mutation,[23,25] or environmental changes.[26] Recent developments in new AFM technologies[13] and magnetic tweezers-based assays[27] greatly enhanced the resolution and the scope of SMFS on membrane protein studies and thus allowed hidden intermediates and the secondary stage of membrane protein folding to be directly observed.

Despite the tremendous contributions of SMFS to the understanding of membrane protein folding,[8,28] AFM-based SMFS has its own limitations in structural mapping and interpretation of unfolding intermediates. The essentially one-dimensional information obtained, *i.e.*, the contour length (L_C), strongly restricts the precision of the structural assignment and limits the microscopic details that can be deduced. The current method for L_C-to-structure mapping typically employed assumptions about: (i) the location of a nonspecific attachment point[9,26] or a reference state,[13] (ii) parameters in polymer models such as the contour length per amino acids unfolded,[9,11−13,15,29] (iii) partially folded states

Received: December 26, 2023
Revised: February 29, 2024
Accepted: March 1, 2024
Published: March 16, 2024

© 2024 The Authors. Published by American Chemical Society

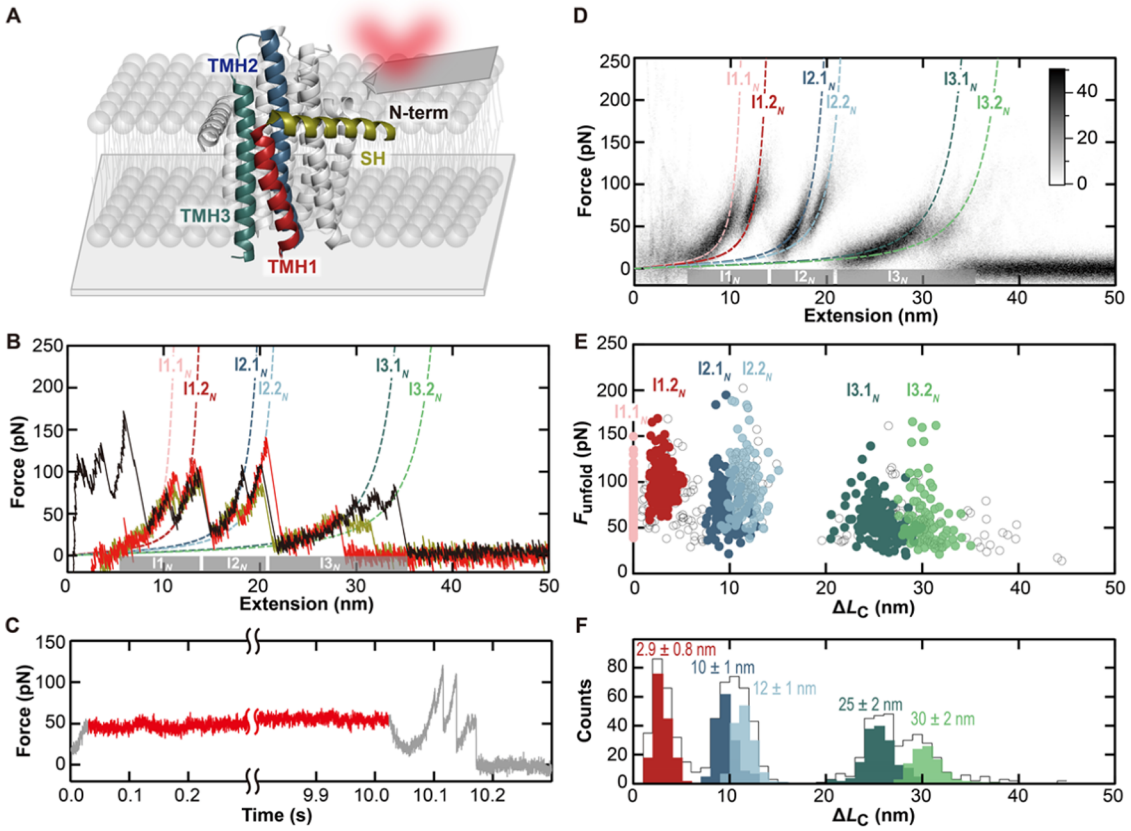

Figure 1. Single-molecule force spectroscopy of DGK unfolding. (A) Cartoon illustrating the unfolding of individual DGK molecules from the reconstituted trimer assembly initiated from the N terminus. (B) Representative FECs showing common signatures of the N-terminal unfolding pathway of DGK. Three groups of force peaks can be readily observed, as labeled by gray bars denoting the relevant extension range of each group. Six major intermediates are denoted by the theoretical curves (colored dashed lines with state labels). (C) Force vs time trace demonstrating that DGK covalently attached to an AFM tip can be held in state $I1.1_N$ at ∼50 pN for 10 s (red) before the molecule was further stretched until complete unfolding. (D) Superpositions of 96 FECs plotted in heat maps, highlighting the population of major intermediates. Scale bars denote the density of the data points in each bin. FECs obtained by site-specific attachment with a longer PEG linker cannot be superimposed together due to the stretching of the extra PEG linker. But common features such as relative positions and the strength of major force peaks can be well reproduced (Figure S3). (E, F) Unfolding force versus contour length plot ($F-\Delta L_C$ plots, (E)) and the contour length histogram (F) showing the relative position and stability of major intermediates. Empty dots and histograms denote statistics of all intermediates observed, and the colored dots and histograms represent data points that were classified into specific major intermediates. The mean contour length changes for major intermediates relative to the first state $I1.1_N$ were labeled (N_{total} = 161). Errors represent the standard deviation.

adopting native conformation, and (iv) fully stretching of the unfolded polypeptide.[12,30] As typically estimated from the standard deviation of L_C, the accuracy for structural assignment of unfolding intermediates of α-helical membrane proteins was around 5−10 amino acids in general.[9,14,26,30] Although a resolution of 2−3 amino acids in the detection of intermediates was achieved by recent technical advances,[13,31] inaccuracy remained in the structure mapping and interpretation of these states without advanced instrumentation or data acquisition schemes, imposing practical limitations on the resolution of actual state identification. In particular, with the improved resolution and an expanded database, more intermediates were found to populate at unconventional locations apart from the ends of transmembrane helices (TMHs); thus, the unfolding pathways do not always correlate with the secondary structure.[9,13,21,26,32] How specific residues or individual physical interactions contribute to the mechanical stability of unfolding intermediates remained largely unknown, hindering the submolecular-level understanding of membrane protein folding.

Complementary to experiments, molecular dynamics (MD) simulations resolve structural dynamics at atomic resolution.[33−35] All-atom simulations have long been used to study the folding/unfolding mechanisms of various membrane proteins and provided extended microscopic insights into experimental observations.[36−41] However, the high computational cost of the conventional all-atom MD simulation makes it impossible to sufficiently equilibrate the intermediate structures and recover the correct pulling process in SMFS. Instead, MD simulations based on coarse-grained models[42,43] could efficiently sample the unfolding pathway and reproduce major experimental observations, including the short-lived unfolding intermediates and their near-equilibrium folding dynamics.

To better elucidate the microscopic mechanism of key interactions stabilizing membrane proteins, it is essential to determine more precisely the stepwise transitions involved in force-induced unfolding. To this end, we examined the mechanical unfolding of *Escherichia coli* diacylglycerol kinase (DGK). DGK is a homotrimeric transmembrane kinase,[44] consisting of three TMHs (TMH1 to TMH3) and one amphipathic surface helix (SH) (Figure 1A). The structure of DGK has been resolved in different membrane environments by X-ray crystallography[45] and nuclear magnetic resonance

https://doi.org/10.1021/jacsau.3c00829
JACS Au 2024, 4, 1422−1435

(NMR) techniques.[46−48] As a classical model for membrane protein folding, DGK was found to exhibit considerable thermodynamic and kinetic stability.[49,50] Over 100 mutations of DGK have been probed, and many of them exhibit defective folding or function.[51−53] But the molecular mechanism for securing its stability or inducing its misfolding is not clear. A comprehensive study of the forced unfolding of DGK provides key information for understanding the physical interactions that govern DGK folding, the molecular determinants of DGK misfolding, and the general mechanism of membrane protein folding.

Here, we used SMFS measurements in combination with multiscale MD simulation approaches to understand the structure transition and the molecular mechanism involved in the mechanical unfolding of DGK. The good agreement between results from simulations and experiments established an excellent rationale to use predictions from simulations to precisely map the locations of intermediates observed in experiments, which could be otherwise difficult to assign by established experimental approaches. All-atom free energy simulations were utilized to identify specific interactions that contribute to the stability of unfolding intermediates and therefore provided mechanistic explanations to the formation of these states. Furthermore, we were able to alter the predicted interaction network by mutagenesis, resulting not only in a significant reduction of the mechanical stability of related intermediates but also in a decrease of the stability of the DGK trimer. Correlated results obtained from SMFS and stability measurements, coarse-grained and all-atom simulations demonstrate connections between the mechano-stability of unfolding intermediates and the molecular determinants of membrane protein stability and therefore provide extra significance beyond existing understanding of the mechanical unfolding of membrane proteins.

RESULTS

Mechanical Unfolding of DGK from the N Terminus

DGK was expressed in *E. coli*, purified by Ni-NTA affinity chromatography, and reconstituted into liposomes.[46,54] Reconstituted DGK formed trimer (Figure S1A) and its functionality was verified by the established activity assay.[44,54] Proteoliposomes containing native DGK were absorbed onto freshly cleaved mica and imaged. AFM topology showed proteoliposomes opened up to form single-layered membrane patches containing densely packed DGK (Figure S1B).

We first conducted SMFS nonspecifically using clean unfunctionalized AFM tips. The AFM tip was pushed onto membrane patches containing unlabeled DGK with a contact force of ∼700 pN for 1 s to facilitate the nonspecific adhesion to the protein. The tip was then retracted by a constant velocity (v = 500 nm/s) and induced unfolding mechanically when a single DGK was attached. The force−extension curves (FECs) recorded the sequence of events in the unfolding pathway of DGK. In principle, unlabeled DGK could adhere to the AFM tip from either the N- or C-terminal end or the periplasmic and cytoplasmic loops (Figure 1A). In practice, after screening for FECs showing force peaks extending over a distance corresponding to the contour length of the fully stretched DGK, representative FECs showed only one major class of unfolding patterns (Figure 1B), indicating one of the termini preferentially attach to the AFM tip via nonspecific adhesion.

To assign from which terminus DGK was unfolded in nonspecific experiments, SMFS was then performed using a site-specific attachment scheme based on the click chemistry[55] to preferentially unfold DGK from one prelabeled end. To do this, DGK labeled at the N-terminal end by dibenzocyclooctyl (DBCO) (Figure S2) was probed by an azide functionalized AFM tip with a reduced contact force of ∼200 pN for 3 s. FECs recorded from the N-terminally labeled DGK reproduced all features observed in nonspecific FECs (Figure S3), suggesting DGK attach predominantly to the AFM tip from the N-terminal end in the nonspecific pulling experiments. We further verified this covalent attaching preference by extensive waiting (∼10 s) at an elevated force (∼50 pN; Figure 1C). Unfunctionalized tips preferentially attach nonspecifically to the N terminus, partly due to a longer N-terminal unstructured loop followed by the surface-exposed helix SH. Alternatively, when DGK was unfolded specifically from the C terminus, a new class of unfolding patterns was observed (Figure S4), exhibiting its own distinct features.

Mechanical Signatures of DGK Unfolding

The superimposition of FECs initiated from the N-terminal end showed three distinct groups of force peaks, denoted by $\mathbf{I1}_N$ to $\mathbf{I3}_N$ (Figure 1D). Each group of force peaks was composed of one or more obligate (with 100% occupancy) or nonobligate (with occupancy <100%) unfolding intermediates. Six major intermediates (with occupancy >50%) from the N-terminal pathway were identified and denoted as $I1.1_N$ (*i.e.*, the first intermediate in group $\mathbf{I1}_N$), $I1.2_N$, *etc.*, two of which ($I1.1_N$ and $I3.1_N$) were observed to be obligate. A full list of intermediates is summarized in Table S1.

To determine the contour length of each state, the unfolding segments from each individual FEC were fitted by polymer models describing the elasticity of unfolded polypeptide chain with or without the poly(ethylene glycol) (PEG) linker[56−58] (Methods Section). The contour length changes ΔL_C between states allowed determination of structural segments unfolded in each step. The unfolding force of each intermediate gives a relative measure of the mechanical stability of each state. The resulting unfolding force versus contour length (F−ΔL_C) plot therefore represents a fingerprint of the unfolding pathway of the protein (Figure 1E,F). The unfolding pathway was dominated by the topology of the protein in the lipid bilayer, similar to other membrane proteins.[21] Roughly speaking, each group of intermediates is likely related to the unfolding of one TMH. However, when trying to map the structure of each intermediate more precisely, contradicted results may appear when using different assumptions about reference states or different choices of model parameters (Figure S5). As common hypotheses in the conventional L_C-to-structure mapping,[9,13,26] either the tip attachment point was assumed to locate at one terminal end of the protein in nonspecific experiments (Figure S5B,C), or major obligate intermediates were assumed to correlate with the topology of the protein in a specific attachment scheme using the PEG linker with variable lengths (Figure S5D,E). In addition, possible inaccuracies in polymer models and the model parameters, such as the contour length per amino acid (reported values ranging from 0.36 to 0.4 nm/aa[9,11−13,15,29]) (Figure S5A) or the persistence length of the unfolded polypeptide[9,13,19,59−63] (Figure S6), may further increase the uncertainties in structural mapping.

https://doi.org/10.1021/jacsau.3c00829
JACS Au 2024, 4, 1422−1435

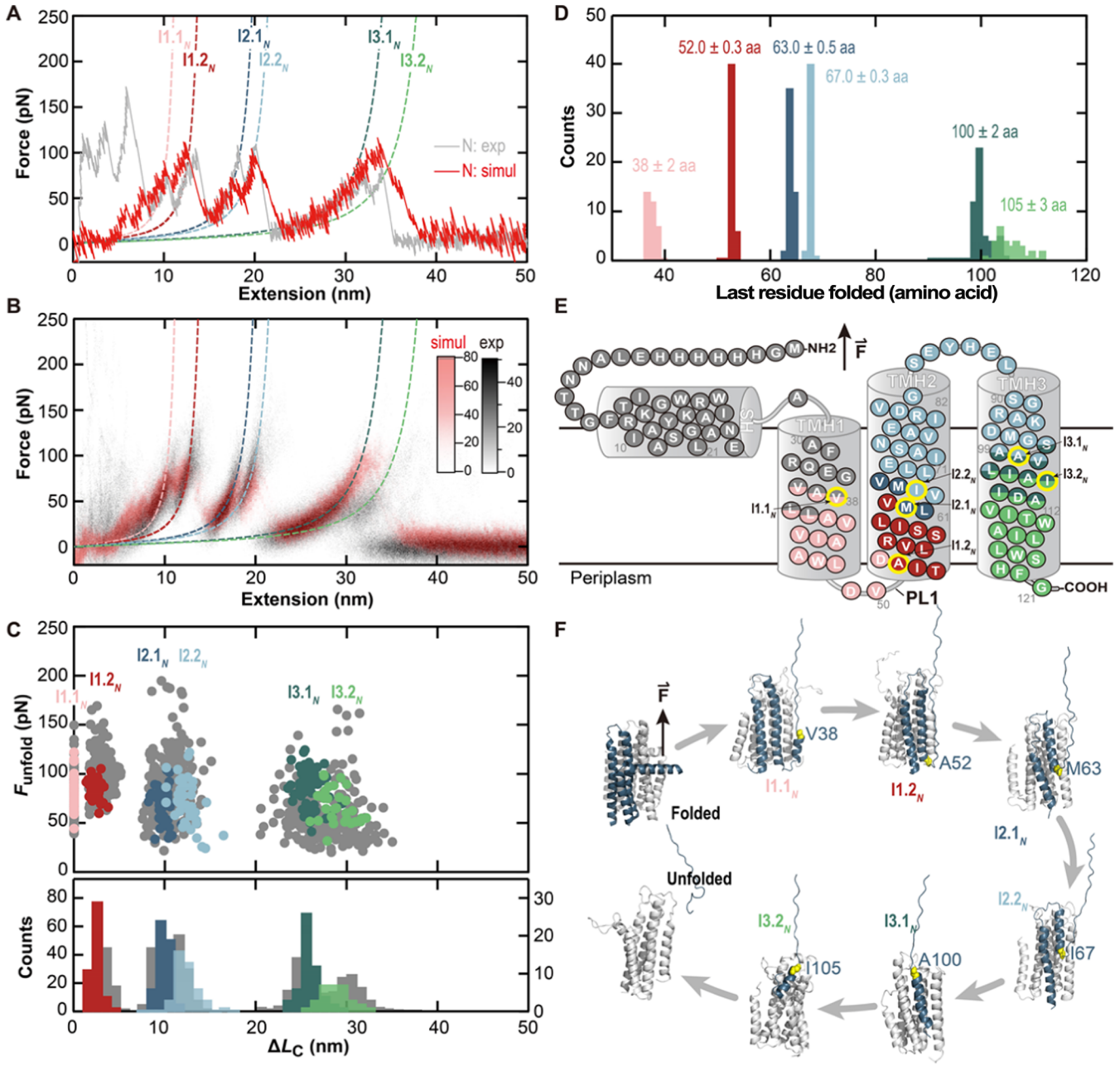

Figure 2. Unfolding pathway and structural assignment of intermediates from coarse-grained simulations. (A) Simulated FEC (red) reproducing major unfolding intermediates observed in experiments (gray). (B) Density plot of superimposed FECs from simulations (red: N_{total} = 56) showing good agreement with experimental traces (gray). (C) $F-\Delta L_C$ plots (top) and the contour length histograms (bottom) of major intermediates determined from simulated FECs (color) compared with experimental results (gray). The contour length changes of most major intermediates from simulations are in good agreement with experiments. (D) Histograms of amino acid positions of major intermediates (last residue remains folded in each state) obtained from simulations showed the positions of states $I1.2_N$, $I2.1_N$, and $I2.2_N$ can be precisely determined with errors less than one amino acid. (E) Positions of major intermediates mapped into the secondary structure of DGK (yellow circle). Each structural segment with filled colors represents the folding unit that stabilizes each major intermediate. Residues with multiple color shades indicate the standard deviations of the boundaries. (F) N-terminal unfolding pathway illustrated as representative snapshots of major intermediates from simulations. TMH1 and TMH3 were extracted from the side of the membrane where the force was applied (the forward-pulling geometry), whereas the unfolding of TMH2 was started from the opposite side (the reverse pulling geometry).

Unfolding Pathway from Coarse-Grained Simulations

We then performed MD simulations to seek more accurate ways of structural assignment and residue-level explanations of the unfolding intermediates. We first employed a recently developed coarse-grained MD simulation algorithm, *Upside*,[42] to characterize the unfolding pathway of DGK. *Upside* uses a physics-based model that simplifies the protein residues by five atoms (N, C_α, C, H, and O) and a side-chain bead and the membrane and the aqueous solution by an implicit solvent model. The energy function includes hydrogen bonds, side chain/side chain and side chain/backbone interactions, and a solvation term. DGK was modeled based on the X-ray structure[45] (PDB code: 3ZE4). Force was applied vertically via a virtual spring attached to the C_α atom of the terminal

https://doi.org/10.1021/jacsau.3c00829
JACS Au 2024, 4, 1422−1435

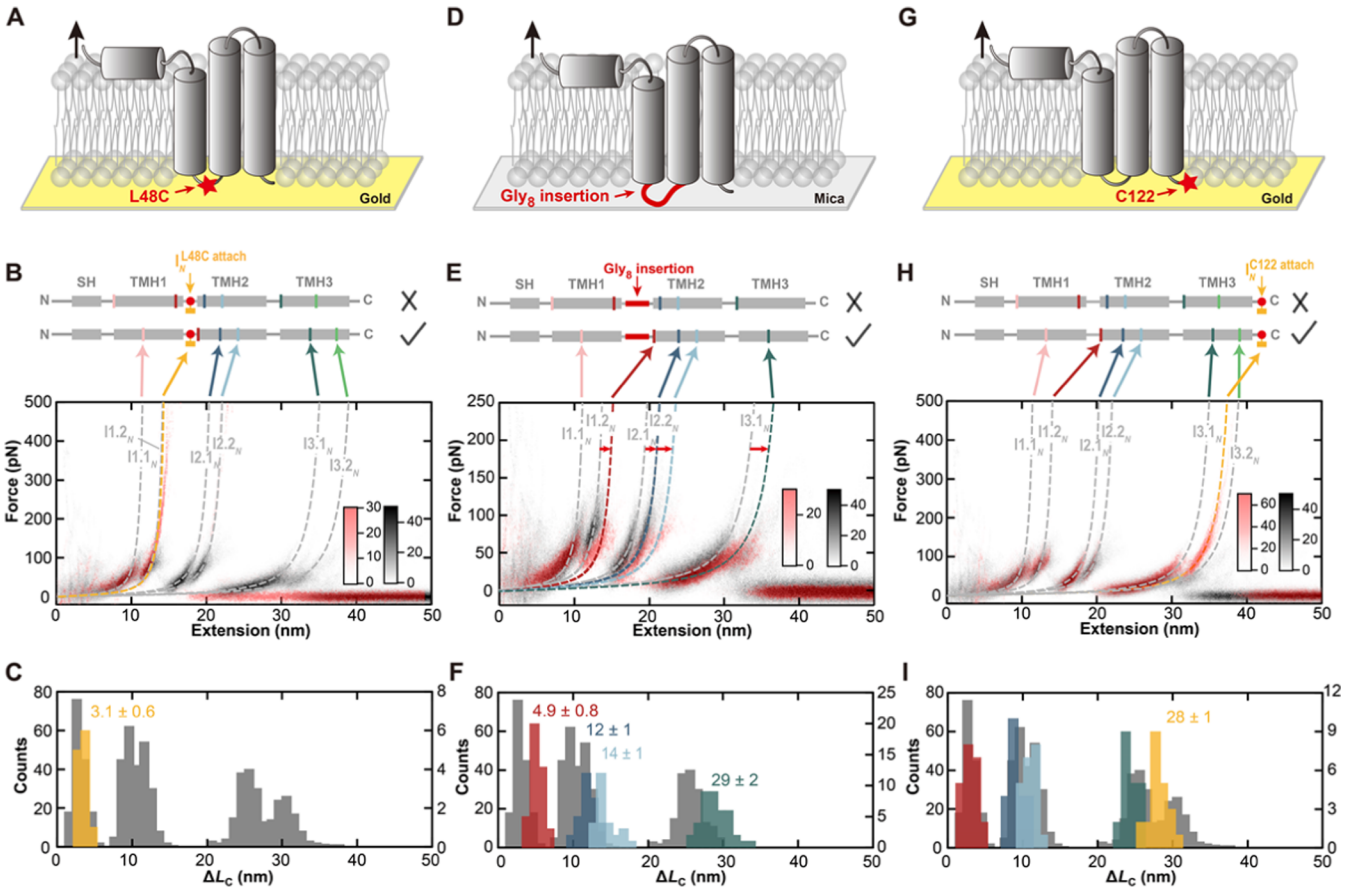

Figure 3. Verification of the structural assignment of unfolding intermediates. The structural assignment based on simulations was examined by three sets of control experiments. (A–C) The L48C mutant was anchored to a gold substrate at Cys48 and unfolded from the N-terminal end (A). The density plot of superimposed FECs (B) and the contour length histogram (C) from L48C (red) and cWT DGK (gray) showed that Cys48 was linked to the gold surface and detached by applying larger unfolding forces (yellow dashed line). The cartoons in B showed one type of plausible positions of intermediates based on conventional assumptions (upper) relative to our state assignments (lower). The fact that the L48C attachment point locates in close proximity to $I1.2_N$ agreed with our state assignment and was inconsistent with the plausible results. (D–F) The periplasmic loop 1 of DGK was elongated by 8 amino acids and the construct was mechanically unfolded from the N terminus (D). The density plot of superimposed FECs (E) and the contour length histogram (F) showed that all intermediates after $I1.2_N$ from the loop-insertion mutant (color dashed lines and histograms) were shifted to a longer extension compared to results from cWT DGK (gray dashed lines and histograms), as expected from our state assignment (cartoons in (E)). (G–I) The C122 mutant was anchored to a gold substrate and unfolded from the N-terminal end (G). The density plot of superimposed FECs (H) and the contour length histogram (I) from C122 and cWT DGK showed the position of the Cys122 surface attachment point (the yellow dashed line and histogram) relative to the major unfolding intermediates (gray dashed lines and histograms). The contour length difference between $I3.1_N$ (Figure 1F) and Cys122 was 3 ± 2 nm, positioning $I3.1_N$ in the middle of TMH3.

residue in one of the subunits. The spring (with spring constant $k = 0.1k_BT/Å^2$ or ∼42 pN/nm) is moved away from the membrane at a constant velocity ($v = 10^{-4}$ nm/step). The slow pulling velocity enabled by *Upside* ensures sufficient relaxation of the partially unfolded protein. Indeed, simulations performed at pulling velocities differing by 3 orders of magnitude showed no quantitative difference in the population of major unfolding intermediates (Figure S7). Although the slowest speed used in simulations is still estimated to be 2 orders of magnitude faster than the highest pulling speed used in our experiments (Methods Section), the essential characteristics of major intermediates reproduced the experimental observations, similar to other proteins tested previously.[42]

FECs from *Upside* simulations aligned well with the experimental results (Figure 2A). To get better statistics and more quantitative comparison, in total of 56 independent simulations were performed. Key features of major unfolding intermediates were recapitulated in all simulations, including the positions and relative unfolding forces (Figure 2B,C). Interestingly, MD simulations based on the solution NMR structure of DGK in detergent micelles[48] (PDB code: 2KDC) deviate from the experimentally observed unfolding behavior with states $I2.1_N$ and $I2.2_N$ not observed (Figure S8), suggesting DGK adopts a native structure in our preparation similar to that resolved by X-ray. This result is consistent with a recent verification by the solid-state NMR that DGK in lipid bilayers showed a global folding similar to that determined by X-ray,[46] and indicates that DGK in detergent micelles may lack key interactions stabilizing the missing unfolding intermediates that are otherwise present in the lipid bilayer environment.

Structural Assignment and Verification of Intermediates

Based on the unfolding process obtained from the MD simulations, we were able to assign structures to the experimentally observed intermediates. To identify intermediate states and their positions from the simulated trajectories, the folding status of each residue was analyzed and the position

https://doi.org/10.1021/jacsau.3c00829
JACS Au 2024, 4, 1422–1435

of the last residue remaining folded in the α-helical conformation was determined for each step. An intermediate was identified when one specific conformation was occupied for long enough time (>50 simulation steps) and the last residue remaining folded in this particular conformation was used to represent the position of the state (Figure S9). The averaged positions of major intermediates determined in this way (Figure 2D) were mapped to the secondary structure of DGK (Figure 2E,F). The boundaries of several states ($I1.2_N$, $I2.1_N$, and $I2.2_N$) can be localized with a single amino acid precision. For example, the $I2.1_N$-to-$I2.2_N$ transition was designated to unfold from Met63 to Ile67, involving the unwinding of just four amino acids or one α-helical turn. Nevertheless, some intermediates exhibit larger errors, indicating possibilities of larger conformational flexibility or the existence of closely spaced states. Interestingly, the width of the contour length distribution of each state obtained from the simulated trajectories remained as large as that of the experimental results (Figure 2C). In contrast, a direct analysis of the population of conformations within each intermediate from simulations, as measured from the distribution of last folded residues (Figure 2D), provides superior precision in structure assignment compared with the traditional protocol based on the analysis of the contour length distribution.

In addition to the superior precision in the state boundary assignment, our coarse-grained simulations also identified the formation of non-native intermediate structures during the unfolding of DGK. We found three different scenarios of non-native conformations from the simulations, with corresponding intermediates observed in SMFS experiments. (i) The unfolded segments may not be fully stretched, forming intermediate helical structures lying on the membrane interface (Figure S10A−C). (ii) TMHs may bend without unfolding when pulled in a reverse pulling geometry, especially in the unfolding of TMH2, leading to extra minor intermediates observed around $I2.1_N$ and $I2.2_N$ (Figure S10D−F). (iii) TMHs may translate vertically within the lipid bilayer without unfolding in the forward-pulling geometry, as observed in the unfolding of TMH1 and TMH3 (Figure S10G−I). The presence of the non-native intermediate states may further conflict with assumptions employed in conventional structural mapping.

Having demonstrated that structures of intermediates can be mapped with high accuracy, we next examined whether the assigned positions reflect actual folding segments that stabilize the protein. Unexpectedly, the boundaries of intermediates identified from simulations (Figure 2E) deviate from the plausible assignments based on conventional assumptions (Figure S5). $I1.1_N$ and $I3.1_N$ were assigned to the middle of TMH1 and TMH3, positioning $I1.2_N$ to the N terminus of TMH2 and $I3.2_N$ close to the end of the protein. To verify the potentially controversial assignment of intermediate structures, we performed additional specifically designed control experiments (Figure 3). First, the positions of $I1.1_N$ and $I1.2_N$ were confirmed by anchoring a single cysteine mutant at L48C in the periplasmic loop 1 (PL1) to a gold substrate (Figure 3A−C) and by elongating PL1 with a poly glycine extension (Figure 3D−F). Both mutants provided anchoring points or extensions at PL1, which is predicted to locate between $I1.1_N$ and $I1.2_N$ in our structural assignment but after $I1.2_N$ based on conventional assumptions. Our results showed that the anchoring point at Cys48 is located in close proximity to $I1.2_N$ (Figure 3B,C), and the loop extension increased the separation between $I1.1_N$ and $I1.2_N$ (Figure 3E,F), in good agreement with our structural assignment. Second, the position of $I3.1_N$ was verified by anchoring the end of TMH3 at the C terminus of the protein (Cys122) to a gold substrate (Figure 3G−I). The wormlike-chain (WLC) fitting revealed a contour length difference of 3 ± 2 nm between $I3.1_N$ and Cys122 (Figure 3I), corresponding to a contour length change of ∼13 amino acids (after taking into account the size of the folded helical structure), suggesting $I3.1_N$ locates closer to the middle of TMH3. Interestingly, the Cys122 surface attachment peak was observed to be 2 ± 2 nm shorter than state $I3.2_N$ (Figure 3H,I), suggesting that the C-terminal segment of TMH3 involves vertical translation within the membrane at the final stage of forced unfolding of free DGK molecules, as observed in the coarse-grained simulations (Figure S10 G−I).

With structures of all major intermediates unambiguously assigned, DGK was found to unfold sequentially, with structural segments varying in size from a few amino acids to half of a helix. The identified unfolding intermediates do not correlate exactly with the secondary structure of DGK, as evidenced primarily by the following two aspects. First, obligate intermediates ($I1.1_N$ and $I3.1_N$) were positioned 5−10 amino acids away from the top of the corresponding helices. For example, $I1.1_N$ was assigned to Val38, whereas TMH1 starts at Ala30. MD simulations revealed that the unfolding of the N-terminal segment of TMH1 occurred at lower forces (Figure S11A). Experimental FECs, when examined carefully, also showed similar early transition events before the unfolding of $I1.1_N$ (Figure S11B). Similarly, the position of $I3.1_N$ at Ala100 also deviates from the top of TMH3 (Ser90), indicating reduced stability of the terminal segment of the corresponding TMHs near the membrane-water interface. Second, additional intermediates with TMH2 resisting forces in a reverse pulling geometry (*i.e.*, $I1.2_N$, $I2.1_N$, $I2.2_N$ in Figure 2F) were highly populated (>90%) and have high mechanical stability. The unfolding forces of these states were comparable to the unfolding forces of two other obligate intermediates ($I1.1_N$ and $I3.1_N$), both from experimental observations (Figure 1E and Table S1) and simulation predictions (Figure 2C). However, in a reverse pulling geometry, TMHs may not resist high stretching forces without extra stabilizing interactions. Such discrepancies between stable folding segments and the secondary structure were also observed in the unfolding of other membrane proteins,[21] but the reason remains unclear. Interestingly, the $I2.1_N$ and $I2.2_N$ states were not observed in simulations unfolding individual DGK monomers (Figure S12) in contrast to the results based on trimeric models (Figure 2), indicating that intermolecular interactions may play a role in stabilizing these states. The high propensity of TMH2 to populate stable intermediates against high reverse pulling forces may suggest a possible novel mechanism with unknown extra interactions that stabilize DGK, which will be probed in the following sections by all-atom simulations and mutagenesis.

Unfolding Mechanism and Interaction Analysis from Free Energy Simulations

To seek for in-depth explanation of the population of unfolding intermediates at unexpected locations and identify key interactions that stabilize the states, we then applied all-atom MD simulations combined with enhanced sampling technique[64,65] to simulate DGK unfolding in an explicit lipid bilayer environment. All-atom simulations provide more

https://doi.org/10.1021/jacsau.3c00829
JACS Au 2024, 4, 1422−1435

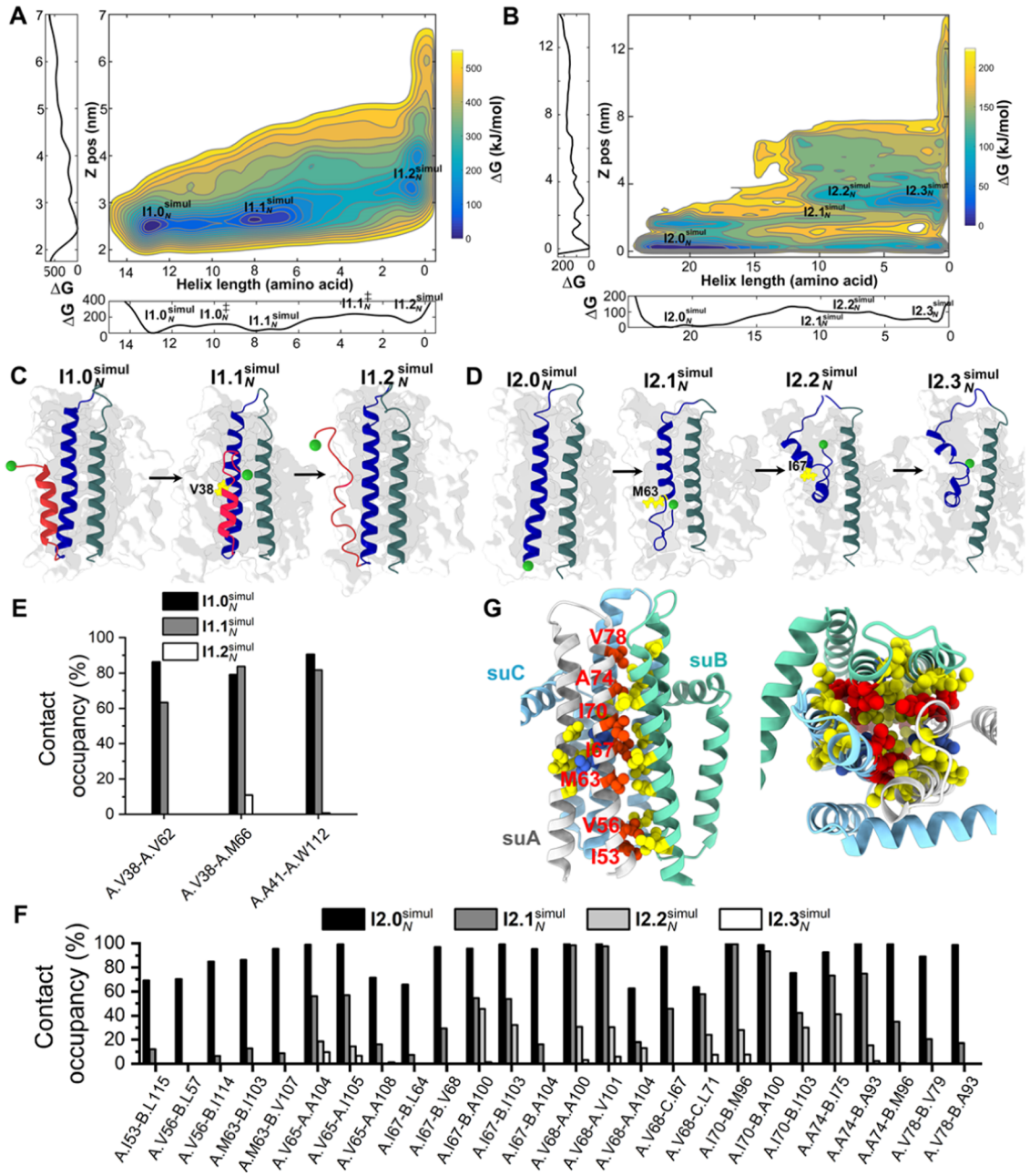

Figure 4. Free energy landscape and interaction analysis from all-atom simulations. (A, B) Two-dimensional FEL for N-terminal unfolding of TMH1 (A) and TMH2 (B) as a function of the helix length and the position of the N-terminal end of the helix (Z). Corresponding one-dimensional free energy profile along a lowest free energy path against each coordinate is shown in the left and bottom panels. (C, D) Representative structures of intermediates observed in the FEL of TMH1 (C, TMH1 in red) and TMH2 (D, TMH2 in blue) unfolding. The subunit being unfolded is shown as ribbon, with the last residue remaining folded in α-helical structure colored yellow and the free end colored light green. The other two subunits are shown as surface in gray. (E) Occupancies of residue−residue contacts within each intermediate observed in the FEL of TMH1 unfolding in (A). A higher contact occupancy indicates the two residues form a stable interaction that may contribute to the stability of the specific intermediate. Here, all three pairs of interactions observe high contact probability in states $I1.0_N^{simul}$ and $I1.1_N^{simul}$, and the residues lose their contact in $I1.2_N^{simul}$, indicating these interactions may contribute to the stability of $I1.1_N^{simul}$. (F) Occupancies of residue−residue contacts within each intermediate observed in the FEL of TMH2 unfolding in *B*. Most interaction pairs observe high contact probability in state $I2.0_N^{simul}$, and lose their contact in the sequential unfolding steps. (G) The identified residues in (F) were plotted on the tertiary structure of DGK. Two critical packing interfaces formed by these apolar residues, one between subunit A (suA, white) and B (suB, green) and the other on the opposite side, can be observed. Constitute residues in TMH2 facing the interface between subunits A and B were shown in red, and the corresponding interaction pairs in B were shown in yellow. Constitute residues in TMH2 facing the opposite side were shown in blue, and the corresponding interaction pairs in subunits A and C (suC, cyan) were shown in yellow.

accurate information about residue contacts that may be missing in coarse-grained models without explicit side chains and membrane lipids. A specially designed simulation protocol (Methods Section) was performed to characterize the unfolding of each TMH separately. To mimic the sequential extraction of TMHs from the N terminus by force, we removed all residues before the N-terminal end of the particular helix being considered and applied biased potential only to the helix

https://doi.org/10.1021/jacsau.3c00829
JACS Au 2024, 4, 1422−1435

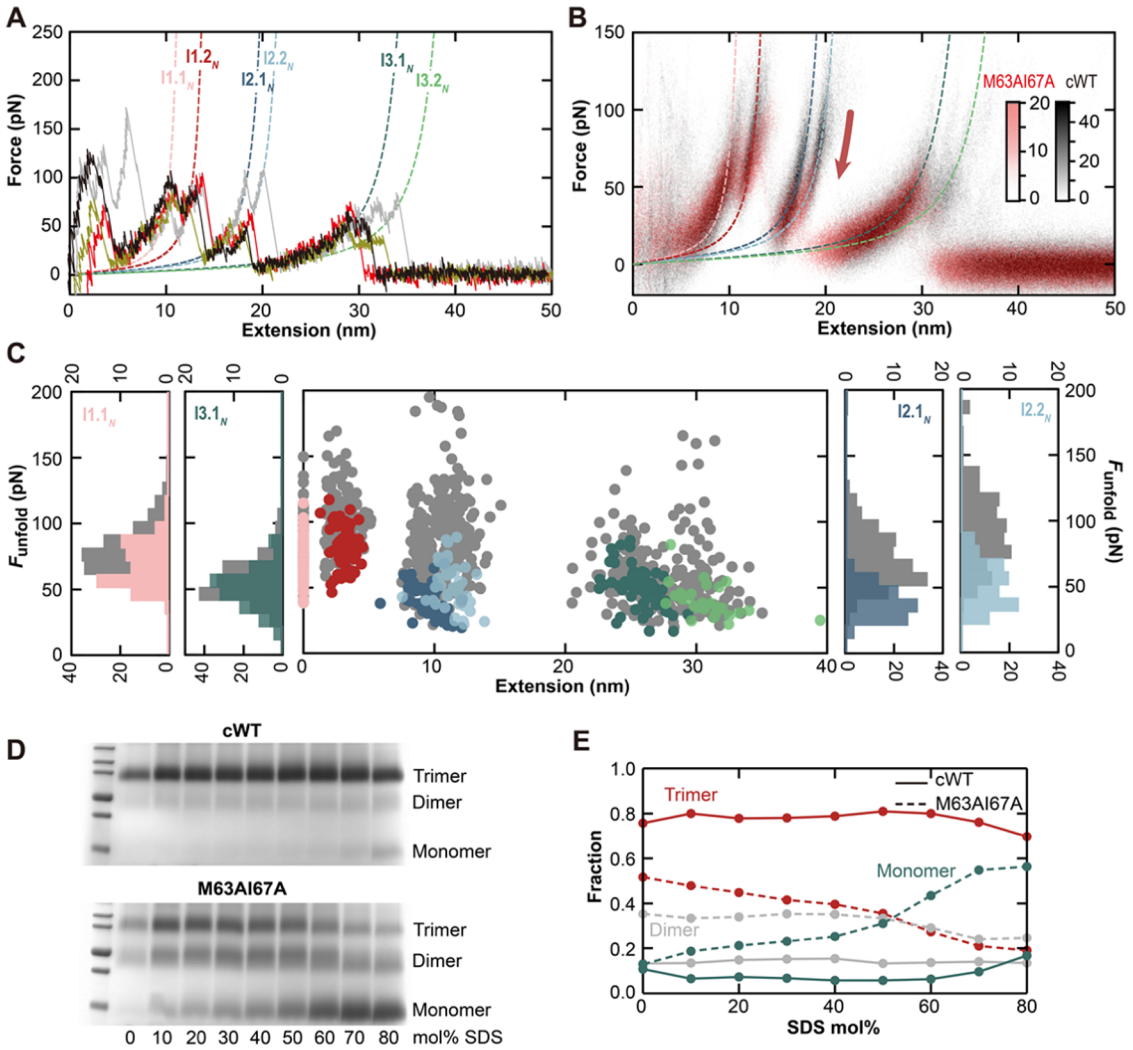

Figure 5. Relative mechano- and thermo-stability of the M63A/I67A mutant. (A) Representative FECs upon N-terminal unfolding of the M63A/I67A mutant (color) plotted in comparison with results from cWT proteins (gray). (B) Density plot of 56 FECs from the M63A/I67A mutant (red) showing destabilization of $I2.1_N$ and $I2.2_N$ (red arrow) compared with results from cWT proteins (gray). (C) F-ΔL_C plot and the unfolding force histogram of representative intermediates showing that the unfolding forces of $I2.1_N$ and $I2.2_N$ were significantly decreased (panels on the right), whereas the unfolding forces of other intermediates ($I1.1_N$ and $I3.1_N$ shown on the left panels) were largely unchanged. (D) cWT DGK (top) or the M63A/I67A mutant (bottom) reconstituted into proteoliposomes titrated with SDS and subjected to glutaraldehyde cross-linking. (E) Fraction of monomeric, dimeric, and trimeric forms of cWT DGK and its mutant under each SDS concentration was determined by analyzing corresponding bands in (D). cWT DGK trimer was highly resistant to SDS up to a molar percentage of 80%. The double mutant formed a trimer without SDS, but disassociated quickly into dimers and monomers at low SDS concentrations.

being unfolded. This allows us to calculate the folding free energy landscape (FEL) for each TMH and analyze key interactions that stabilize the observed intermediates.

The two-dimensional FEL for unfolding TMH1 and TMH2 from the N terminus was plotted as a function of the helix length and the position (Z) of the free end of the helix (Figure 4A,B). Multiple metastable states can be readily observed from the local minima of the FEL. The unfolding pathway of a given helix can be then identified by characterizing a lowest free energy path from the fully folded state to the fully extended state passing multiple energy minima and valleys. Intermediates detected from the free energy simulations (Figure 4C,D) recapitulate major intermediates observed in the SMFS experiments and the coarse-grained simulations. In addition, individual interactions between residues that contribute to the stability of these intermediates can be also determined by analyzing the occupancy of contacts between pairs of residues within each energy minimum observed on the FEL (Methods Section). Residue pairs with high contact probability were identified that lose their interaction as unfolding proceeds (Figure 4E,F), indicating the two residues form a stable interaction that may contribute to the stability of the specific intermediate.

The FELs obtained from the all-atom enhanced sampling simulations provide explanations for the unusual unfolding behavior of the DGK observed in experiments. Indeed, the reduced mechanical stability of the N-terminal segment of TMH1 and the resulted deviation of $I1.1_N$ from the very top of the helix could be readily understood. Based on the FEL and the one-dimensional free energy profiles (Figure 4A), unfolding of TMH1 was found to proceed in two major steps. TMH1 first unfolds from fully folded state $I1.0_N^{simul}$, crossing the barrier $I1.0_N^{\ddagger}$, to first intermediate $I1.1_N^{simul}$, in which helical structures up to Val38 are unfolded. Then, a

https://doi.org/10.1021/jacsau.3c00829
JACS Au 2024, 4, 1422−1435

higher barrier $I1.1_N^{\ddagger}$ compared to $I1.0_N^{\ddagger}$ must overcome to unfold $I1.1_N^{simul}$. Contact analysis revealed that this rate-limiting step involves the breaking of side-chain interactions between Val38 and Ala41 in TMH1 with Val62 and Met66 in TMH2 and Trp112 in TMH3 (Figure 4E). The existence of these extra pairs of intramolecular interactions generated a higher barrier to unfold $I1.1_N^{simul}$. As a result, a mechanically stable state that required higher forces to unfold occurs at Val38, whereas the lower first barrier $I1.0_N^{\ddagger}$ results in low-force unfolding of the N-terminal segment of TMH1.

More importantly, the microscopic basis of the impact of specific residue−residue interactions on the stability of each intermediate can be determined from the FEL analysis. We particularly focus on interactions involving TMH2, and seek understanding of the molecular determinants of the unusually stable intermediates at the reverse pulling geometry, *i.e.*, $I1.2_N$, $I2.1_N$, and $I2.2_N$. We found that side-chain packing mediated by a large number of hydrophobic residue pairs is essential for stabilizing these states (Figure 4F). Particularly, residues in TMH2A, including Ile53, Val56, Met63, Ile67, Ile70, Ala74, and Val78 (Figure 4G, red residues), participated in intermolecular interactions with partners from subunit B (Figure 4G, yellow residues in suB). Geometrically, these apolar side chains in TMH2A are facing outward to the interface between the adjacent subunits and are separated mostly by one α-helical turn (Figure 4G). This interaction network stabilizes the three major intermediates, $I1.2_N$ at Ala52, $I2.1_N$ at Met63, and $I2.2_N$ at Ile67, and one minor intermediate at Val56 observed in both experiments and the coarse-grained simulations (Figure S13). The positions of the four states coincide with the first four constituting residues in TMH2A that contribute to the packing interactions. After the unfolding of Ile67, the interaction network could be largely destabilized, and no more metastable state exists. In addition to the strong packing interface between subunit A and B, the opposite face of TMH2A (Figure 4G, blue residues) also forms a second critical area of packing with TMH3A and TMH2C (Figure 4G, yellow residues in suA and suC). These findings suggest that the hydrophobic side chains, when facing the interface, are contributing to the high stability of the DGK trimer. The higher mechanical stability of the unexpectedly stable intermediates $I1.2_N$, $I2.1_N$, and $I2.2_N$ is directly related to the distinct tight intermolecular packing of DGK assembly.

Effect of M63A/I67A on the Mechano- and Thermo-Stability

To examine the impact of intermolecular interactions on the stability of the mechanical unfolding intermediates and the trimeric assembly of DGK as predicted by simulations, two alanine mutations were introduced at the Met63 and Ile67 positions. These two sites were identified as the locations of the two special intermediates $I2.1_N$ and $I2.2_N$, and were also predicted to participate key intermolecular interactions that stabilize these states. We hypothesized that the M63A/I67A variation might induce packing defects into the side-chain interaction network, weaken interactions between TMH2A, TMH2B, and TMH3B, thus reducing the mechanical stability of $I2.1_N$ and $I2.2_N$, and also reducing the stability of the DGK trimer.

The influence of the double alanine mutations on the mechanical stability of the DGK unfolding intermediates was first determined by SMFS. DGK carrying M63A/I67A mutations were expressed, purified, and reconstituted by the same procedures as the cysteine-modified variant of the wild-type protein (cWT DGK). M63A/I67A mutants were unfolded from the N-terminal end and the resulting FECs were superimposed with FECs from cWT proteins (Figure 5A,B). We found that the positions of all major unfolding intermediates of M63A/I67A were identical to those detected in cWT proteins. But the unfolding forces of $I2.1_N$ and $I2.2_N$ were significantly reduced, while the unfolding forces of other major intermediates were barely changed (Figure 5C). Combining these results showing a significant reduction of the mechanical stability of $I2.1_N$ and $I2.2_N$ upon mutation (Figure 5), along with the coarse-grained simulations showing the complete elimination of the two states when unfolding individual DGK monomers (Figure S12), our findings verified the dominant role of the intermolecular interactions in stabilizing these mechanical unfolding intermediates.

We then examined the effect of the double mutations on the relative thermodynamic stability of the DGK trimer. Reconstituted proteoliposomes containing cWT and M63A/I67A proteins were destabilized by various amounts of sodium dodecyl sulfate (SDS) and cross-linked with glutaraldehyde.[51] The trimeric, dimeric, and monomeric fraction as a function of SDS concentration was then determined by SDS-polyacrylamide gel electrophoresis (PAGE) (Figure 5D,E). The cWT DGK exhibited high stability, resisting high concentration of SDS (up to 80%). The M63A/I67A mutant formed trimer without SDS, but was unstable and quickly dissociated into dimers and monomers even at low concentrations of SDS. Overall, these results confirmed that the intermolecular interactions revealed by MD simulations were crucial for both the mechano-stability of corresponding intermediates and also the thermo-stability of DGK trimer.

DISCUSSION

The molecular mechanisms of membrane protein folding are of broad interest. Although mechanical unfolding by AFM-based SMFS has been used for over 20 years to explore the principles of membrane protein folding and function,[12] the microscopic basis of each unfolding step remained controversial.[21] Here we combined force spectroscopy with multiscale simulations and mutagenesis to study the pathway and mechanism of DGK unfolding. We were able to achieve robust and precise structural assignments to major unfolding intermediates and understand their molecular determinants. Unfolding transitions involving structural changes of four amino acids or one α-helical turn can be well resolved and assigned to a precision of a single amino acid. We find apolar side-chain packing constructed by an intermolecular network of hydrophobic residues as the major contribution to the special intermediates observed in our experiments with TMHs resisting high forces in the reverse pulling geometry. The relation between the high mechano-stability of unfolding intermediates and the high thermo-stability of the DGK trimer was therefore established via the identification of this tight interaction network.

Traditionally in SMFS, the putative structures of unfolding intermediates were inferred from a direct mapping of contour length changes into the secondary structure.[21] The boundaries of folding segments determined in this way may observe large systematic or random errors,[30] partly due to possible uncertainties in the chosen reference state.[9,13,26] Given the disagreement between our state assignment (Figure 2E) and the plausible results based on conventional assumptions (Figure S5), extra care should be taken when using the

https://doi.org/10.1021/jacsau.3c00829
JACS Au 2024, 4, 1422−1435

terminal end of the protein or the top of helices as the guidance in state assignment. Since the nonspecific adhesion could in principle happen at any exposed positions near the terminus, the averaged attachment point may deviate from the very end of the protein. Extra verification or guidance from simulations or control experiments is necessary. In addition, uncertainties in model parameters used (Figures S5 and S6) and the formation of non-native structures in both the folded and unfolded segments of the partially unfolded protein (Figure S10) may further affect the accuracy of structural mapping. At least three different scenarios for forming non-native conformations during DGK unfolding were observed in our SMFS experiments and simulations (Figure S10). All three cases involve global movement of partially folded helical segments within or at the surface of the lipid bilayer, and could also result in noncooperative hump transitions in the unfolding of DGK (Figure S14) and other membrane proteins.[15] The unfolding humps occurred infrequently (11%) in FECs taken from the cWT DGK, but they can become significantly more pronounced in the unfolding of the M63A/I67A mutant (42%). This increased propensity of movements of folded helical segments also suggests reduced helix−helix interactions upon mutation, in agreement with our interaction analysis.

DGK was found to have high stability,[49,50] whereas many of its mutants were misfolding prone or functional defective.[51,52] How inter- and intramolecular interactions contribute to maintain its stability and how these interactions were tuned by mutations leading to misfolding remained unclear. Our result showed that mutations at the trimer interface disrupt intermolecular interactions and cause significant destabilization of the DGK trimer. Two packing interfaces, one between TMH2A, TMH2B, and TMH3B, the other between TMH2A, TMH3A, and TMH2C, are used to solidify the inter- and intrahelical assembly of this protein. Among the many types of forces that stabilize membrane proteins, this interaction network lacks charged, polar, or aromatic residues that participate in charge−charge, hydrogen bonding, or aromatic−aromatic interactions. We performed energy decomposition analysis[66] and found attractive van der Waals interactions were present between the predicted interacting residue pairs (Figure S15). Thus, in a bilayer environment where the hydrophobic effect is not contributing to folding,[1,2,5] the global stability of DGK folding is mainly dominated by the dense van der Waals packing resulting from interactions between hydrophobic residues at the helix−helix interface. This finding also supports the previous hypothesis that stabilizing contributions from the interface is providing a high level of stability of DGK[50] and other membrane protein oligomers.[5,67,68] When packing defects were created by mutations, the helix−helix interactions and the trimeric assembly were destabilized.

In summary, our results highlight the experiment-simulation combined approach is potentially a more precise way for structural assignment and can provide a detailed molecular-level description of membrane protein folding. A key feature of this study is the demonstration of a frequently under-appreciated relation between the mechano-stability of unfolding intermediates from vertical pulling experiments and the underlying microscopic basis of interhelical interactions that is orthogonal to the pulling axis. The high stability of DGK was found to be secured largely from a network of weak van der Waals interactions that can be tuned by mutations. These findings further offer applications in the general understanding of the currently poorly elucidated misfolding mechanism of membrane proteins.[3] The destabilizing mechanisms discovered here may offer explanations to one type of frequently observed disease-causing mutations that induce misfolding by disrupting helix−helix interactions.[3] This approach, complementary to other recent efforts in developing new methodologies for deciphering submolecular details of membrane proteins from SMFS,[15,23,24,27,40,41] may provide fundamentally new insights into understanding membrane protein folding and misfolding.

METHODS

DGK Expression, Purification, and Reconstitution

The plasmid of DGK was generously provided by Prof. Jun Yang. The construct harbors a His_6 tag at the N terminus for purification and one cysteine at either the N-terminal (N3C-DGK) or the C-terminal (C122-DGK) end for site-specific modification. All internal cysteines of DGK were mutated (C46A, C113A). These single cysteine variants were referred to as cWT DGK in our work, which allowed DBCO functionalization at one specific terminus. Other mutations were generated based on the cWT DGK construct by PCR-based site-directed mutagenesis. The sequence of all DGK variants used in this work is shown in Table S2. cWT DGK or the mutants were expressed in BL21 Star (DE3) competent *E. coli* cells and purified by Ni-NTA Superflow agarose (Thermo Scientific) as previously described.[46]

To label the protein with DBCO, we first reduced the terminal cysteine by incubating the protein with 10 mM tris(2-carboxyethyl)-phosphine (TCEP) for 3 h at room temperature. The sample was buffer exchanged into the coupling buffer (20 mM sodium phosphate buffer (NaPi), pH 7.2, 0.2% SDS) using centrifugal filters with a 10 kDa cutoff. DGK was then incubated with DBCO-PEG_4-maleimide or DBCO-PEG_n-maleimide (molecular weight (M_W) = 5000 Da) at a molar ratio of 1:1 to 30:1 for 24 h at room temperature. The free DBCO was removed by dialysis or a buffer exchange. The labeling efficiency was assessed by SDS-PAGE (Figure S2).

Reconstitution of DGK was performed following existing protocols, with minor modifications.[54] Briefly, purified cWT DGK or its variants were mixed with 1-palmitoyl-2-oleoyl-*sn*-glycero-3-phosphocholine (POPC) micelles containing 50 mM POPC and 200 mM dodecylphosphocholine (DPC) in water at lipid-to-protein ratios of 50:1 to 120:1. The mixture was incubated on the rotator at room temperature overnight and then transferred into a dialysis tubing with a molecular weight cutoff of 10 kDa (Spectra-Por, Spectrum). The sample was dialyzed for 7−14 days at 18 °C against the dialysis buffer (20 mM NaPi, pH 6.6, 0.5 mM ethylenediaminetetraacetic acid (EDTA)), which was changed twice per day.

Activity Assay

The activity of DGK reconstituted into proteoliposomes was monitored using the established assay.[44,54] Briefly, the assay was prepared by adding 10 μL of 50 mM nicotinamide adenine dinucleotide (NADH) and 50 μL of 1000 U/mL pyruvate kinase/lactic dehydrogenase (PK/LDH) (Sigma-Aldrich) into 440 μL of the assay mix containing 75 mM piperazine-*N*,*N*′-bis (2-ethanesulfonic acid) (PIPES), 50 mM LiCl, 0.1 mM ethylene glycol-bis (β-aminoethyl)-*N*,*N*,*N*′,*N*′-tetraacetic acid (EGTA), 0.1 mM EDTA, 21 mM *n*-dodecyl-β-maltoside (DM), 3 mM cardiolipin (Avanti), 3 mM dibutyrin (DBG) (Macklin), 20 mM adenosine triphosphate (ATP), 55 mM $MgCl_2$, 1 mM phosphoenolpyruvate, monopotassium salt (PEP-K), and 1 mM TCEP, pH 6.8. Then, 5 μL of reconstituted DGK stock (∼0.1−1 mg/mL) was added and transferred into a 96-well microplate. The decrease of absorbance at 340 nm as a result of NADH oxidation was recorded using a microplate reader (Molecular Devices FlexStation 3).

Single-Molecule Force Spectroscopy Assay

To prepare DGK samples for force spectroscopy, we diluted the reconstituted DGK to ∼10 ng/μL in the absorption buffer (10 mM Tris, 300 mM KCl), and deposited 50 μL onto freshly cleaved mica. After 1 h, the mica surface was rinsed extensively by the phosphate-

https://doi.org/10.1021/jacsau.3c00829
JACS Au 2024, 4, 1422−1435

buffered saline (PBS) (137 mM NaCl, 2.7 mM KCl, 10 mM Na_2HPO_4, and 1.8 mM KH_2PO_4, pH 7.2). All measurements were performed in PBS.

DGK carrying single cysteine mutations at L48C or Cys122 was directly linked to the gold substrate via thiol-Au bonds. To prepare DGK attached to the gold substrate, a gold-coated silicon wafer was prepared by ultrasonic cleaning in isoproposol and water, respectively, for 5 min and then oxidized by soaking it in H_2O_2 for 12 h. Oxidized wafers were again treated with ultrasonic cleaning in water 3 times and blow-dried with nitrogen. Finally, the protein sample was deposited within 5 min of surface preparation. After 1 h incubation, the gold surface was rinsed extensively by PBS.

We measured the unfolding of DGK using BioLever mini cantilevers (AC40TS, Olympus) in a commercial AFM (Cypher ES, Asylum Research). To specifically attach the AFM tip to one prelabeled end of DGK, the cantilevers were functionalized using protocols developed previously.[55,69] Briefly, cantilevers were first rinsed in toluene, isopropanol, and deionized water and then activated using a UV ozone system. We then incubated the cantilevers in the toluene solution of silane-PEG$_n$-azide (0.15 mg/mL) at 60 °C for 3 h. Two different lengths of PEG linkers were used (M_W = 600 or 3400 Da). Cantilevers were finally rinsed in toluene, isopropanol, and deionized water again and stored in a humidity chamber at 4 °C.

Analysis of Force−Extension Curves

To screen out multiple tethers or partial unfolding, the contour length change from the first major state to the last major state (ΔL_C^{last}) was used as a criterion. Traces with ΔL_C^{last} = 20−50 nm were included in our analysis. Further inspection based on common unfolding features excluded an additional ∼20% of traces.

To determine the contour length of each state, we fit each segment of FECs associated with major intermediate states with proper models describing the elasticity of the stretched polypeptide chain and the PEG linker. For the nonspecific FECs and the simulated traces, only the unfolded polypeptide was stretched. An improved approximation of the WLC model was used to analyze these curves[56,58]

$$F(x) = \frac{k_B T}{L_p}\left[\frac{1}{4}\left(1 - \frac{x}{L_c}\right)^{-2} - \frac{1}{4} + \frac{x}{L_c} - \frac{4}{5}\left(\frac{x}{L_c}\right)^{2.15}\right] \quad (1)$$

where L_p is the persistence length (0.4 nm) of the polypeptide and k_BT is the thermal energy. For specific FECs, we fit each state using two components in series. The first part describes the elasticity of the unfolded polypeptide using eq 1. The second part uses the freely jointed chain to model the elasticity of the PEG linker[57]

$$L(F) = N_S\left[\frac{L_{planar}}{e^{-\Delta G/k_BT} + 1} + \frac{L_{helical}}{e^{\Delta G/k_BT} + 1}\right]\cdot \left[\coth\left(\frac{F\cdot L_K}{k_BT}\right) - \frac{k_BT}{F\cdot L_K}\right] + N_S\cdot\frac{F}{K} \quad (2)$$

where N_S is the total number of PEG segments, L_{planar} is the contour length of a PEG monomer in the *ttt* state (0.28 nm), $L_{helical}$ is the contour length of a PEG monomer in the *ttg* state (0.358 nm), ΔG is the free energy difference between the two conformations (3 k_BT), L_K is the Kuhn length, and K is the enthalpic stretch modulus. Global fitting was performed to determine the contour lengths of all major intermediates identified, and an average change of contour lengths for these states was reported in Figure 1 and Table S1.

Stability Measurements of the DGK Trimer

The relative thermodynamic stability was determined by a cross-linking/SDS-PAGE assay.[51] Reconstituted DGK in POPC vesicles was first equilibrated in 75 mM PIPES, 50 mM LiCl, 0.1 mM EGTA, 0.1 mM EDTA, and 12 mM DM, pH 6.9. Samples were then titrated using SDS to concentrations ranging from 0 to 80% (mol/mol). The molar concentration of SDS was calculated by [SDS]/([SDS] + [DM] + [POPC]). 32 mM glutaraldehyde was added to the mixture for cross-linking overnight and the sample was analyzed by 12% SDS-PAGE. Protein band intensities were quantified using ImageJ.

Upside Simulations of DGK Unfolding

The *Upside* simulations were performed using the simulation package from Wang et. al.[42] With a near all-atom representation of membrane proteins and implicit models of solvent and membranes, *Upside* is efficient and completes each simulation replica of the unfolding process of DGK within 1−2 days' time on a single CPU-core. With an implicit membrane, the lipid−protein interactions are described by the level of residue side-chain immersed in lipids and calculated based on a knowledge-based membrane burial potential.[42]

The structure of DGK was adopted from the Protein Data Bank. The position of DGK relative to the membrane was predicted by Positioning of Proteins in Membranes (PPM) 2.0 Web Server.[70] Springs were attached to the C_α atom of the N-terminal residue. The pulling forces were added in the direction perpendicular to the membrane surface. The spring constant was set to be 0.1 $k_BT/Å^2$ (∼42 pN/nm at 300 K) and the standard pulling velocity was 10^{-4} nm/step. The estimation of the real time scale of the *Upside* simulation remained controversial, as pointed out by Wang et. al.[42] A simulation velocity of 0.001 Å/step was estimated to be ∼10^6 nm/s.[42] Although this value is still 2 orders of magnitude higher than the fastest pulling speed used in experiments, the characteristics of unfolding pathway, including the population and unfolding forces of unfolding intermediates, match well with experimental results. The discrepancy of speed values used in experiments and simulations could be due to unknown errors in the conversion of the simulation time step to the real time, or other inaccuracies in the energy function.[42]

Free Energy Simulations of DGK Unfolding

The all-atomic MD simulations combined with enhanced sampling techniques were employed to investigate the free energy of unfolding intermediates and identify key interactions that stabilize these states. The free energy simulations were performed in an explicit lipid bilayer environment with explicit solutions. To simulate the sequential unfolding of each TMH, the protein segment unfolded prior to the relevant helix was truncated. For example, to study the unfolding of TMH1 from the N-terminal end, residues from the N terminus of the protein up to Ala29 (before the N terminus of TMH1) were removed, and the rest of the protein was inserted into the lipid bilayer composed of 200 POPC molecules. In the simulation, the bias potential was added only to the helix considered to enhance the unfolding of the particular helix. Sodium and chlorine ions were added to neutralize the system and the final concentration of sodium chloride was set to be 150 mM. The charmm36 force field was employed for the proteins and the membrane[71] and the TIP3P model was used for water molecules.[72] All bonds related to hydrogen atoms were constrained with the LINCS algorithm.[73] An isotropic scheme was utilized to couple the lateral and perpendicular pressures separately. The Particle-Mesh Ewald method[74] was employed to calculate long-range electrostatics with a cutoff of 10 Å. The temperatures were coupled with the Nose−Hoover method[75] and the pressures were coupled by a Parrinello−Rahman barostat.[76] To obtain the free energy landscapes of each TMH, we employed the well-tempered metadynamics simulations[77] to sample the conformations in the unfolding/folding process. The estimation of free energy at time t as a function of the collective variables (CVs) s was determined by the following formula

$$F(s, t) = -\frac{T + \Delta T}{\Delta T}V(s, t) \quad (3)$$

where $V(s,t)$ is the biased potential deposited on the system and ΔT is the difference between the fictitious temperature of the CV and the temperature of the simulation, which tunes the height of the biased potential in the simulation. The vertical position of the N-terminal end (Z) and the helicity of the corresponding helices were employed as the two CVs in the metadynamics simulation. The initial height of the Gaussian potential is 1 kJ/mol and deposited every 5 ps. The bias

https://doi.org/10.1021/jacsau.3c00829
JACS Au 2024, 4, 1422−1435

factor was set to be 16. For the free energy sampling of different helices, 200 to 600 ns production runs were performed with 2 fs time step by GROMACS2019.[78]

Contact Analysis

Contacts between residues were defined as the residue pairs that are close within a distance threshold (4.5 Å for any heavy atom pairs in these two residues) in the protein conformation. The occupancy of residue−residue contacts measures the ratio of conformations to the contacted residue pairs in each intermediate. The occupancy of contacts between residue i and j in state s is defined as

$$O_{i,j}^{s} = \frac{\sum_{t}^{N_s} \delta_{i,j}^{t}}{N_s} \quad (4)$$

where $\delta_{i,j}^{t} = 1$ if the residues i and j are in contact with each other in conformation t, otherwise it equals 0. N_s is the conformation number in state s. Here, the intermediate states are defined based on the free energy minima on the FEL, and all of the conformations belonging to the state are utilized to perform the contact analysis.

■ ASSOCIATED CONTENT

Supporting Information

The Supporting Information is available free of charge at https://pubs.acs.org/doi/10.1021/jacsau.3c00829.

Reconstituted DGK and site-specific attachment scheme; additional FECs from the N or C terminus; plausible structural mapping of intermediates based on conventional assumptions; simulated FECs using different pulling velocities, the NMR structure or the monomeric DGK; analysis of simulated FECs; nonnative intermediate structures observed during the unfolding of DGK; noncooperative unfolding humps; list of major unfolding intermediates and their structural parameters; and sequences of DGK constructs (PDF)

■ AUTHOR INFORMATION

Corresponding Authors

Mojie Duan − *Innovation Academy for Precision Measurement Science and Technology, Chinese Academy of Sciences, Wuhan 430071, China;* orcid.org/0000-0002-5496-832X; Email: mjduan@wipm.ac.cn

Hao Yu − *School of Physics, Huazhong University of Science and Technology, Wuhan 430074, China;* orcid.org/0000-0003-1589-7781; Email: hyu@hust.edu.cn

Authors

Huiying Yang − *School of Physics, Huazhong University of Science and Technology, Wuhan 430074, China*

Daihong Zhou − *School of Physics, Huazhong University of Science and Technology, Wuhan 430074, China*

Zhangyi Zhou − *School of Physics, Huazhong University of Science and Technology, Wuhan 430074, China*

Complete contact information is available at: https://pubs.acs.org/10.1021/jacsau.3c00829

Author Contributions

H.Y. conceived the project. M.D. performed the simulations. H.Y., D.Z., and H.Y. performed the experiments. H.Y., Z.Z., M.D., and H.Y. analyzed the data and produced the figures. All authors wrote the paper. CRediT: **Huiying Yang** data curation, formal analysis, investigation, methodology, writing-review & editing; **Daihong Zhou** data curation, formal analysis, methodology, writing-review & editing; **Zhangyi Zhou** data curation, formal analysis, writing-review & editing; **Mojie Duan** data curation, formal analysis, funding acquisition, investigation, methodology, writing-review & editing; **Hao Yu** conceptualization, data curation, formal analysis, funding acquisition, investigation, project administration, supervision, writing-original draft, writing-review & editing.

Funding

This work was supported by the National Natural Science Foundation of China [grant nos. 11774107, 12174132, and 31971157 (to H.Y.), and grant no. 21773298 (to M.D.)].

Notes

The authors declare no competing financial interest.

■ ACKNOWLEDGMENTS

The authors thank Prof. Jun Yang and Dr. Yanke Chen for providing plasmids and protocols for preparing DGK samples, and Prof. Tom Perkins for helpful discussions.

■ REFERENCES

(1) Corin, K.; Bowie, J. U. How physical forces drive the process of helical membrane protein folding. *EMBO Rep.* **2022**, *23* (3), No. e53025.

(2) Hong, H. Toward understanding driving forces in membrane protein folding. *Arch. Biochem. Biophys.* **2014**, *564*, 297−313.

(3) Marinko, J. T.; Huang, H.; Penn, W. D.; Capra, J. A.; Schlebach, J. P.; Sanders, C. R. Folding and Misfolding of Human Membrane Proteins in Health and Disease: From Single Molecules to Cellular Proteostasis. *Chem. Rev.* **2019**, *119* (9), 5537−5606.

(4) Fiedler, S.; Broecker, J.; Keller, S. Protein folding in membranes. *Cell. Mol. Life Sci.* **2010**, *67* (11), 1779−1798.

(5) Mravic, M.; Thomaston, J. L.; Tucker, M.; Solomon, P. E.; Liu, L.; DeGrado, W. F. Packing of apolar side chains enables accurate design of highly stable membrane proteins. *Science* **2019**, *363* (6434), 1418−1423.

(6) DeGrado, W. F.; Gratkowski, H.; Lear, J. D. How do helix−helix interactions help determine the folds of membrane proteins? Perspectives from the study of homo-oligomeric helical bundles. *Protein Sci.* **2003**, *12* (4), 647−665.

(7) Stanley, A. M.; Fleming, K. G. The process of folding proteins into membranes: challenges and progress. *Arch. Biochem. Biophys.* **2008**, *469* (1), 46−66.

(8) Bippes, C. A.; Muller, D. J. High-resolution atomic force microscopy and spectroscopy of native membrane proteins. *Rep. Prog. Phys.* **2011**, *74* (8), No. 086601.

(9) Spoerri, P. M.; Kato, H. E.; Pfreundschuh, M.; Mari, S. A.; Serdiuk, T.; Thoma, J.; Sapra, K. T.; Zhang, C.; Kobilka, B. K.; Müller, D. J. Structural Properties of the Human Protease-Activated Receptor 1 Changing by a Strong Antagonist. *Structure* **2018**, *26* (6), 829−838.e824.

(10) Harris, N. J.; Pellowe, G. A.; Blackholly, L. R.; Gulaidi-Breen, S.; Findlay, H. E.; Booth, P. J. Methods to study folding of alpha-helical membrane proteins in lipids. *Open Biol.* **2022**, *12* (7), No. 220054.

(11) Maity, S.; Mazzolini, M.; Arcangeletti, M.; Valbuena, A.; Fabris, P.; Lazzarino, M.; Torre, V. Conformational rearrangements in the transmembrane domain of CNGA1 channels revealed by single-molecule force spectroscopy. *Nat. Commun.* **2015**, *6*, No. 7093.

(12) Oesterhelt, F.; Oesterhelt, D.; Pfeiffer, M.; Engel, A.; Gaub, H. E.; Muller, D. J. Unfolding pathways of individual bacteriorhodopsins. *Science* **2000**, *288* (5463), 143−146.

(13) Yu, H.; Siewny, M. G. W.; Edwards, D. T.; Sanders, A. W.; Perkins, T. T. Hidden dynamics in the unfolding of individual bacteriorhodopsin proteins. *Science* **2017**, *355* (6328), 945−950.

(14) Kawamura, S.; Gerstung, M.; Colozo, A. T.; Helenius, J.; Maeda, A.; Beerenwinkel, N.; Park, P. S.; Muller, D. J. Kinetic,

energetic, and mechanical differences between dark-state rhodopsin and opsin. *Structure* **2013**, *21* (3), 426−437.
(15) Galvanetto, N.; Ye, Z.; Marchesi, A.; Mortal, S.; Maity, S.; Laio, A.; Torre, V. Unfolding and identification of membrane proteins in situ. *eLife* **2022**, *11*, No. e77427.
(16) Muller, D. J. AFM: A Nanotool in Membrane Biology. *Biochemistry* **2008**, *47* (31), 7986−7998.
(17) Rief, M.; Gautel, M.; Oesterhelt, F.; Fernandez, J. M.; Gaub, H. E. Reversible unfolding of individual titin immunoglobulin domains by AFM. *Science* **1997**, *276* (5315), 1109−1112.
(18) Fernandez, J. M.; Li, H. Force-clamp spectroscopy monitors the folding trajectory of a single protein. *Science* **2004**, *303* (5664), 1674−1678.
(19) Junker, J. P.; Ziegler, F.; Rief, M. Ligand-dependent equilibrium fluctuations of single calmodulin molecules. *Science* **2009**, *323* (5914), 633−637.
(20) Lee, G.; Abdi, K.; Jiang, Y.; Michaely, P.; Bennett, V.; Marszalek, P. E. Nanospring behaviour of ankyrin repeats. *Nature* **2006**, *440* (7081), 246−249.
(21) Kedrov, A.; Janovjak, H.; Sapra, K. T.; Muller, D. J. Deciphering molecular interactions of native membrane proteins by single-molecule force spectroscopy. *Annu. Rev. Biophys. Biomol. Struct.* **2007**, *36*, 233−260.
(22) Janovjak, H.; Struckmeier, J.; Hubain, M.; Kedrov, A.; Kessler, M.; Muller, D. J. Probing the energy landscape of the membrane protein bacteriorhodopsin. *Structure* **2004**, *12* (5), 871−879.
(23) Jacobson, D. R.; Perkins, T. T. Free-energy changes of bacteriorhodopsin point mutants measured by single-molecule force spectroscopy. *Proc. Natl. Acad. Sci. U.S.A.* **2021**, *118* (13), No. e2020083118.
(24) Yu, H.; Jacobson, D. R.; Luo, H.; Perkins, T. T. Quantifying the Native Energetics Stabilizing Bacteriorhodopsin by Single-Molecule Force Spectroscopy. *Phys. Rev. Lett.* **2020**, *125* (6), No. 068102.
(25) Sapra, K. T.; Balasubramanian, G. P.; Labudde, D.; Bowie, J. U.; Muller, D. J. Point mutations in membrane proteins reshape energy landscape and populate different unfolding pathways. *J. Mol. Biol.* **2008**, *376* (4), 1076−1090.
(26) Serdiuk, T.; Madej, M. G.; Sugihara, J.; Kawamura, S.; Mari, S. A.; Kaback, H. R.; Muller, D. J. Substrate-induced changes in the structural properties of LacY. *Proc. Natl. Acad. Sci. U.S.A.* **2014**, *111* (16), E1571−1580.
(27) Choi, H.-K.; Min, D.; Kang, H.; Shon, M. J.; Rah, S.-H.; Kim, H. C.; Jeong, H.; Choi, H.-J.; Bowie, J. U.; Yoon, T.-Y. Watching helical membrane proteins fold reveals a common N-to-C-terminal folding pathway. *Science* **2019**, *366* (6469), 1150−1156.
(28) Jefferson, R. E.; Min, D.; Corin, K.; Wang, J. Y.; Bowie, J. U. Applications of Single-Molecule Methods to Membrane Protein Folding Studies. *J. Mol. Biol.* **2018**, *430* (4), 424−437.
(29) Ainavarapu, S. R. K.; Brujić, J.; Huang, H. H.; Wiita, A. P.; Lu, H.; Li, L.; Walther, K. A.; Carrion-Vazquez, M.; Li, H.; Fernandez, J. M. Contour Length and Refolding Rate of a Small Protein Controlled by Engineered Disulfide Bonds. *Biophys. J.* **2007**, *92* (1), 225−233.
(30) Kessler, M.; Gaub, H. E. Unfolding barriers in bacteriorhodopsin probed from the cytoplasmic and the extracellular side by AFM. *Structure* **2006**, *14* (3), 521−527.
(31) Jacobson, D. R.; Uyetake, L.; Perkins, T. T. Membrane-Protein Unfolding Intermediates Detected with Enhanced Precision Using a Zigzag Force Ramp. *Biophys. J.* **2020**, *118* (3), 667−675.
(32) Serdiuk, T.; Sugihara, J.; Mari, S. A.; Kaback, H. R.; Muller, D. J. Observing a lipid-dependent alteration in single lactose permeases. *Structure* **2015**, *23* (4), 754−761.
(33) Bottaro, S.; Lindorff-Larsen, K. Biophysical experiments and biomolecular simulations: A perfect match? *Science* **2018**, *361* (6400), 355−360.
(34) Milles, L. F.; Schulten, K.; Gaub, H. E.; Bernardi, R. C. Molecular mechanism of extreme mechanostability in a pathogen adhesin. *Science* **2018**, *359* (6383), 1527−1533.
(35) Melo, M. C. R.; Bernardi, R. C. Fostering discoveries in the era of exascale computing: How the next generation of supercomputers empowers computational and experimental biophysics alike. *Biophys. J.* **2023**, *122* (14), 2833−2840.
(36) Stansfeld, P. J.; Sansom, M. S. P. Molecular Simulation Approaches to Membrane Proteins. *Structure* **2011**, *19* (11), 1562−1572.
(37) Flood, E.; Boiteux, C.; Lev, B.; Vorobyov, I.; Allen, T. W. Atomistic Simulations of Membrane Ion Channel Conduction, Gating, and Modulation. *Chem. Rev.* **2019**, *119* (13), 7737−7832.
(38) Lu, W.; Schafer, N. P.; Wolynes, P. G. Energy landscape underlying spontaneous insertion and folding of an alpha-helical transmembrane protein into a bilayer. *Nat. Commun.* **2018**, *9* (1), No. 4949.
(39) Gaffney, K. A.; Guo, R.; Bridges, M. D.; Muhammednazaar, S.; Chen, D.; Kim, M.; Yang, Z.; Schilmiller, A. L.; Faruk, N. F.; Peng, X.; Jones, A. D.; Kim, K. H.; Sun, L.; Hubbell, W. L.; Sosnick, T. R.; Hong, H. Lipid bilayer induces contraction of the denatured state ensemble of a helical-bundle membrane protein. *Proc. Natl. Acad. Sci. U.S.A.* **2022**, *119* (1), No. e2109169119.
(40) Laskowski, P. R.; Pluhackova, K.; Haase, M.; Lang, B. M.; Nagler, G.; Kuhn, A.; Muller, D. J. Monitoring the binding and insertion of a single transmembrane protein by an insertase. *Nat. Commun.* **2021**, *12* (1), No. 7082.
(41) Serdiuk, T.; Manna, M.; Zhang, C.; Mari, S. A.; Kulig, W.; Pluhackova, K.; Kobilka, B. K.; Vattulainen, I.; Müller, D. J. A cholesterol analog stabilizes the human β2-adrenergic receptor nonlinearly with temperature. *Sci. Signalling* **2022**, *15* (737), No. eabi7031.
(42) Wang, Z.; Jumper, J. M.; Freed, K. F.; Sosnick, T. R. On the Interpretation of Force-Induced Unfolding Studies of Membrane Proteins Using Fast Simulations. *Biophys. J.* **2019**, *117* (8), 1429−1441.
(43) Yamada, T.; Yamato, T.; Mitaku, S. Forced Unfolding Mechanism of Bacteriorhodopsin as Revealed by Coarse-Grained Molecular Dynamics. *Biophys. J.* **2016**, *111* (10), 2086−2098.
(44) Van Horn, W. D.; Sanders, C. R. Prokaryotic diacylglycerol kinase and undecaprenol kinase. *Annu. Rev. Biophys.* **2012**, *41*, 81−101.
(45) Li, D.; Lyons, J. A.; Pye, V. E.; Vogeley, L.; Aragao, D.; Kenyon, C. P.; Shah, S. T.; Doherty, C.; Aherne, M.; Caffrey, M. Crystal structure of the integral membrane diacylglycerol kinase. *Nature* **2013**, *497* (7450), 521−524.
(46) Li, J.; Shen, Y.; Chen, Y.; Zhang, Z.; Ma, S.; Wan, Q.; Tong, Q.; Glaubitz, C.; Liu, M.; Yang, J. Structure of membrane diacylglycerol kinase in lipid bilayers. *Commun. Biol.* **2021**, *4* (1), No. 282.
(47) Möbius, K.; Kazemi, S.; Güntert, P.; Jakob, A.; Heckel, A.; Becker-Baldus, J.; Glaubitz, C. Global response of diacylglycerol kinase towards substrate binding observed by 2D and 3D MAS NMR. *Sci. Rep.* **2019**, *9* (1), No. 3995.
(48) Van Horn, W. D.; Kim, H.-J.; Ellis, C. D.; Hadziselimovic, A.; Sulistijo, E. S.; Karra, M. D.; Tian, C.; Sönnichsen, F. D.; Sanders, C. R. Solution Nuclear Magnetic Resonance Structure of Membrane-Integral Diacylglycerol Kinase. *Science* **2009**, *324* (5935), 1726−1729.
(49) Lau, F. W.; Bowie, J. U. A method for assessing the stability of a membrane protein. *Biochemistry* **1997**, *36* (19), 5884−5892.
(50) Jefferson, R. E.; Blois, T. M.; Bowie, J. U. Membrane proteins can have high kinetic stability. *J. Am. Chem. Soc.* **2013**, *135* (40), 15183−15190.
(51) Mi, D.; Kim, H. J.; Hadziselimovic, A.; Sanders, C. R. Irreversible misfolding of diacylglycerol kinase is independent of aggregation and occurs prior to trimerization and membrane association. *Biochemistry* **2006**, *45* (33), 10072−10084.
(52) Wen, J.; Chen, X.; Bowie, J. U. Exploring the allowed sequence space of a membrane protein. *Nat. Struct. Biol.* **1996**, *3* (2), 141−148.
(53) Nagy, J. K.; Sanders, C. R. Destabilizing mutations promote membrane protein misfolding. *Biochemistry* **2004**, *43* (1), 19−25.
(54) Gorzelle, B. M.; Nagy, J. K.; Oxenoid, K.; Lonzer, W. L.; Cafiso, D. S.; Sanders, C. R. Reconstitutive refolding of diacylglycerol kinase, an integral membrane protein. *Biochemistry* **1999**, *38* (49), 16373−16382.

https://doi.org/10.1021/jacsau.3c00829
JACS Au 2024, 4, 1422−1435

(55) Yu, H.; Heenan, P. R.; Edwards, D. T.; Uyetake, L.; Perkins, T. T. Quantifying the Initial Unfolding of Bacteriorhodopsin Reveals Retinal Stabilization. *Angew. Chem.* **2019**, *131* (6), 1724−1727.
(56) Marko, J. F.; Siggia, E. D. Stretching DNA. *Macromolecules* **1995**, *28* (26), 8759−8770.
(57) Oesterhelt, F.; Rief, M.; Gaub, H. E. Single molecule force spectroscopy by AFM indicates helical structure of poly(ethyleneglycol) in water. *New J. Phys.* **1999**, *1*, No. 6.
(58) Petrosyan, R. Improved approximations for some polymer extension models. *Rheol. Acta* **2017**, *56* (1), 21−26.
(59) Avellaneda, M. J.; Franke, K. B.; Sunderlikova, V.; Bukau, B.; Mogk, A.; Tans, S. J. Processive extrusion of polypeptide loops by a Hsp100 disaggregase. *Nature* **2020**, *578* (7794), 317−320.
(60) Ma, L.; Cai, Y.; Li, Y.; Jiao, J.; Wu, Z.; O'Shaughnessy, B.; De Camilli, P.; Karatekin, E.; Zhang, Y. Single-molecule force spectroscopy of protein-membrane interactions. *eLife* **2017**, *6*, No. e30493.
(61) Ott, W.; Jobst, M. A.; Bauer, M. S.; Durner, E.; Milles, L. F.; Nash, M. A.; Gaub, H. E. Elastin-like Polypeptide Linkers for Single-Molecule Force Spectroscopy. *ACS Nano* **2017**, *11* (6), 6346−6354.
(62) Shank, E. A.; Cecconi, C.; Dill, J. W.; Marqusee, S.; Bustamante, C. The folding cooperativity of a protein is controlled by its chain topology. *Nature* **2010**, *465* (7298), 637−640.
(63) Stirnemann, G.; Giganti, D.; Fernandez, J. M.; Berne, B. J. Elasticity, structure, and relaxation of extended proteins under force. *Proc. Natl. Acad. Sci. U.S.A.* **2013**, *110* (10), 3847−3852.
(64) Valsson, O.; Tiwary, P.; Parrinello, M. Enhancing Important Fluctuations: Rare Events and Metadynamics from a Conceptual Viewpoint. *Annu. Rev. Phys. Chem.* **2016**, *67* (1), 159−184.
(65) Bussi, G.; Laio, A. Using metadynamics to explore complex free-energy landscapes. *Nat. Rev. Phys.* **2020**, *2* (4), 200−212.
(66) Miller, B. R.; McGee, T. D., Jr.; Swails, J. M.; Homeyer, N.; Gohlke, H.; Roitberg, A. E. MMPBSA.py: An Efficient Program for End-State Free Energy Calculations. *J. Chem. Theory. Comput.* **2012**, *8* (9), 3314−3321.
(67) Deeds, E. J.; Bachman, J. A.; Fontana, W. Optimizing ring assembly reveals the strength of weak interactions. *Proc. Natl. Acad. Sci. U.S.A.* **2012**, *109* (7), 2348−2353.
(68) Lu, W.; Chai, Q.; Zhong, M.; Yu, L.; Fang, J.; Wang, T.; Li, H.; Zhu, H.; Wei, Y. Assembling of AcrB Trimer in Cell Membrane. *J. Mol. Biol.* **2012**, *423* (1), 123−134.
(69) Walder, R.; LeBlanc, M. A.; Van Patten, W. J.; Edwards, D. T.; Greenberg, J. A.; Adhikari, A.; Okoniewski, S. R.; Sullan, R. M. A.; Rabuka, D.; Sousa, M. C.; Perkins, T. T. Rapid Characterization of a Mechanically Labile alpha-Helical Protein Enabled by Efficient Site-Specific Bioconjugation. *J. Am. Chem. Soc.* **2017**, *139* (29), 9867−9875.
(70) Lomize, A. L.; Todd, S. C.; Pogozheva, I. D. Spatial arrangement of proteins in planar and curved membranes by PPM 3.0. *Protein Sci.* **2022**, *31* (1), 209−220.
(71) Best, R. B.; Zhu, X.; Shim, J.; Lopes, P. E. M.; Mittal, J.; Feig, M.; MacKerell, A. D., Jr. Optimization of the Additive CHARMM All-Atom Protein Force Field Targeting Improved Sampling of the Backbone ϕ, ψ and Side-Chain χ1 and χ2 Dihedral Angles. *J. Chem. Theory Comput.* **2012**, *8* (9), 3257−3273.
(72) Price, D. J.; Brooks, C. L., III. A modified TIP3P water potential for simulation with Ewald summation. *J. Chem. Phys.* **2004**, *121* (20), 10096−10103.
(73) Hess, B.; Bekker, H.; Berendsen, H. J. C.; Fraaije, J. G. E. M. LINCS: A linear constraint solver for molecular simulations. *J. Comput. Chem.* **1997**, *18* (12), 1463−1472.
(74) Essmann, U.; Perera, L.; Berkowitz, M. L.; Darden, T.; Lee, H.; Pedersen, L. G. A smooth particle mesh Ewald method. *J. Chem. Phys.* **1995**, *103* (19), 8577−8593.
(75) Nosé, S. A unified formulation of the constant temperature molecular dynamics methods. *J. Chem. Phys.* **1984**, *81* (1), 511−519.
(76) Parrinello, M.; Rahman, A. Polymorphic transitions in single crystals: A new molecular dynamics method. *J. Appl. Phys.* **1981**, *52* (12), 7182−7190.
(77) Bonomi, M.; Parrinello, M. Enhanced Sampling in the Well-Tempered Ensemble. *Phys. Rev. Lett.* **2010**, *104* (19), No. 190601.
(78) Berendsen, H. J. C.; van der Spoel, D.; van Drunen, R. GROMACS: A message-passing parallel molecular dynamics implementation. *Comput. Phys. Commun.* **1995**, *91* (1), 43−56.

https://doi.org/10.1021/jacsau.3c00829
JACS Au 2024, 4, 1422−1435